Published by :
http://www.ijert.org

International Journal of Engineering Research & Technology (IJERT)
ISSN: 2278-0181
Vol. 14 Issue 06, June - 2025

Design and Performance Observation of Frequency Reconfigurable Multiband Antenna for wireless applications

Akanksha Ladha, Archana Agrawal,
Sangam University, Bhilwara (Rajasthan), India

Ritesh Kumar Saraswat
M.L.V. Textile & Engineering College, Bhilwara (Rajasthan), India

ABSTRACT
This article introduces a slotted multiband antenna incorporating an octagonal-shaped split-ring resonator and a slotted defected ground section with switchable inverted L- and T-shaped stubs. A PIN diode is embedded within the stubs in the defected ground section, enabling frequency-band reconfigurability for diverse wireless communication applications. The proposed antenna resonates at six distinct frequency bands corresponding to key wireless standards: Upper S band at 3.3 GHz for Worldwide Interoperability for Microwave Access (WiMAX); Lower C band at 5.0/5.8 GHz for Wireless Local Area Network (WLAN); 5G Sub-6 GHz NR frequency ranges, specifically n46 and n47; Lower X band at 9.98 GHz for satellite communication; Upper X band at 11.01 GHz for amateur radio applications; and Lower Ku band at 12.07 GHz for molecular rotational spectroscopy. With compact dimensions of 44 × 39 × 1.6 mm³, the antenna is fabricated on an FR4 substrate to validate its simulated performance against measured results. It exhibits consistent radiation characteristics, gain, and efficiency across its resonant bands, making it suitable for multi-standard wireless applications. The design achieves an optimized peak gain of 4.14 dBi and a radiation efficiency of 87.88%.

Keywords: **5G Sub-6 GHz NR Bands, Frequency-band reconfigurable, PIN- diode, Slotted octagonal radiating patch, Wi-MAX , WLAN.**

1. INTRODUCTION

The rapid advancement of wireless communications has accelerated the demand for 5G (fifth-generation) mobile technology, which is defined by features such as high data rates, reduced latency, improved energy efficiency, lower costs, and increased system capacity [1]. Within 5G mobile communication, the Sub-6 GHz band is designated to support various New Radio (NR) bands, offering significant enhancements over 4G networks. The 5G frequency spectrum is divided into two segments: frequencies below 6 GHz (FR1 NR bands) and frequencies above 30 GHz (FR2 bands) for wireless applications [2]. The transition from 4G to 5G has driven extensive research into planar multiband antenna designs [3–5]. Among these, frequency reconfigurable antennas for Sub-6 GHz 5G and WLAN applications remain a prominent focus, with various design methodologies highlighted in [3]. For instance, a magneto-electric dipole antenna offering broadband performance and a high front-to-back ratio (FBR) is detailed in [4], while [5] proposes a wideband multiple-input multiple-output (MIMO) antenna array to improve bandwidth and compatibility with 5G NR bands for mobile devices. Multiband functionality in antenna designs is often achieved through advanced techniques such as slotting, metamaterial loading, and innovative feeding mechanisms [6–15]. In [16], a slot-antenna array with wideband performance and high isolation was developed on an FR4 substrate to cover the 5G NR bands N77, N78, and N79. Similarly, [17] proposed a dual-band, low-profile, quad-port printed antenna for 5G applications, designed to operate within the 3.3–3.8 GHz spectrum (N77 band) with a 10 dB impedance bandwidth, meeting critical requirements for fifth-generation wireless communication. The multi-unit wideband MIMO antenna array approach has proven effective for mobile devices, enhancing bandwidth and ensuring compatibility with 5G NR communication bands [18–20]. Studies [21, 13] report on metamaterial-inspired multiband frequency reconfigurable antennas. Specifically, [21] presents a frequency reconfigurable metamaterial-loaded triple-band antenna designed for WLAN and WiMAX applications. In [13], a six-resonating-band antenna featuring a vertex-fed configuration is introduced, demonstrating frequency reconfigurability tailored for wireless standards. A slot-antenna array designed on an FR4 substrate provides wideband operation and high isolation, supporting multiple resonating bands while achieving enhanced gain and bandwidth [22–26].

Additionally, [23] investigates a stubs-loaded, polarization-switchable single-band antenna, extending its

International Journal of Engineering Research & Technology (IJERT)
ISSN: 2278-0181
Vol. 14 Issue 06, June - 2025

functionality to achieve polarization switching across three frequency bands. The antenna supports LHCP, LP, and RHCP characteristics across all switchable bands. In [24], a compact patch antenna capable of both frequency and polarization reconfigurability is proposed. This design incorporates a square patch with truncated corners and a triangular slot at its center, utilizing PIN diodes and appropriate biasing to enable diverse operating modes. Reference [25] presents an antenna offering frequency and polarization reconfigurability through an open-stub cascaded branch-line coupler (OSCBLC) feed network that employs varactor diodes. Similarly, [26] introduces a compact, frequency-tunable antenna for 4G and 5G conformal portable devices, achieving reconfigurability through slots on the radiating elements and ground plane, leveraging partial and defected ground structures. In [27], a frequency reconfigurable monopole microstrip patch antenna is developed for wireless communication applications. This design supports both single-band and dual-band modes, controlled by the diode switching configuration, and incorporates a multilayer frequency-selective surface (FSS) reflector to enhance gain. Finally, [28] focuses on a wearable dual-band frequency reconfigurable patch antenna for WBAN (Wireless Body Area Network) applications, integrating a PIN diode. To ensure compatibility with WBAN standards, the antenna's Specific Absorption Rate (SAR) values are evaluated using a human tissue model. These SAR values comply with FCC (Federal Communications Commission) and ICNIRP (International Commission on Non-Ionizing Radiation Protection) guidelines for resonating modes with 1/10 g human tissue.

This paper presents a novel octagonal-shaped slotted hexa-band antenna, featuring a slotted SRR-based radiating section and a rectangular partial ground plane with T-shaped and double inverted L-shaped stubs. The antenna is designed to support multiple wireless standards, including WiMAX, WLAN, 5G Sub-6 GHz NR bands, upper C band, lower X band, upper X band, and lower Ku band. The design incorporates an octagonal SRR-based metallic ring integrated with a rectangular slotted radiating section, along with a PIN diode positioned between the T-shaped and inverted L-shaped stubs on the ground plane. The proposed antenna demonstrates frequency reconfigurable capabilities for wireless communication applications, resonating at WiMAX (3.3 GHz), WLAN (5.0/5.8 GHz), 5G Sub-6 GHz NR (n46: 5.15-5.925 GHz, n47: 5.855-5.925 GHz), upper C band (6.76 GHz), lower X band (9.98 GHz), upper X band (11.01 GHz), and lower Ku band (12.07 GHz).

2. DESIGN AND ANALYSIS OF PROPOSED MULTIBAND ANTENNA

This section begins with the design evolution of the proposed SRR-based T- and inverted L-shaped stub-loaded hexa-band antenna. Initially, an octagonal-shaped radiating patch antenna measuring 44 × 39 × 1.6 mm^3 is designed, referred to as Antenna Design 'A' in Figure 1. This configuration operates in a tetra-band mode, resonating at 5.6/7.2/10.6/15.3 GHz, catering to multiple wireless standards. Next, a single split-ring resonator (SRR) is integrated with the radiating section, along with a slotted rectangular feedline. This modification, shown as Antenna Design 'B' in Figures 1 and 2, enables triple-band operation at 5.7/6.8/10.9 GHz. Simulations and performance evaluations were carried out using CST Microwave Studio (MWS) [33]. Further enhancement is achieved by adding another SRR to the radiating section, resulting in Antenna Design 'C' in Figure 1. This configuration achieves penta-band operation, covering 3.3/4.9/5.7/6.7/10.01 GHz for various wireless applications, as illustrated in Figure 2. Finally, T-shaped and double inverted L-shaped stubs are implemented in the ground plane, with a single PIN diode inserted between the stubs. This configuration, labeled Antenna Design 'D' in Figure 1, achieves hexa-band characteristics for wireless applications in the diode's OFF state. The proposed design resonates at 3.3/5.0/5.8/6.8/9.9/11.01/12.05 GHz, as depicted in Figure 2, covering a wide range of wireless communication standards. Table 1 presents the various characteristics of the antenna design across design stages A to D.

International Journal of Engineering Research & Technology (IJERT)
ISSN: 2278-0181
Vol. 14 Issue 06, June - 2025

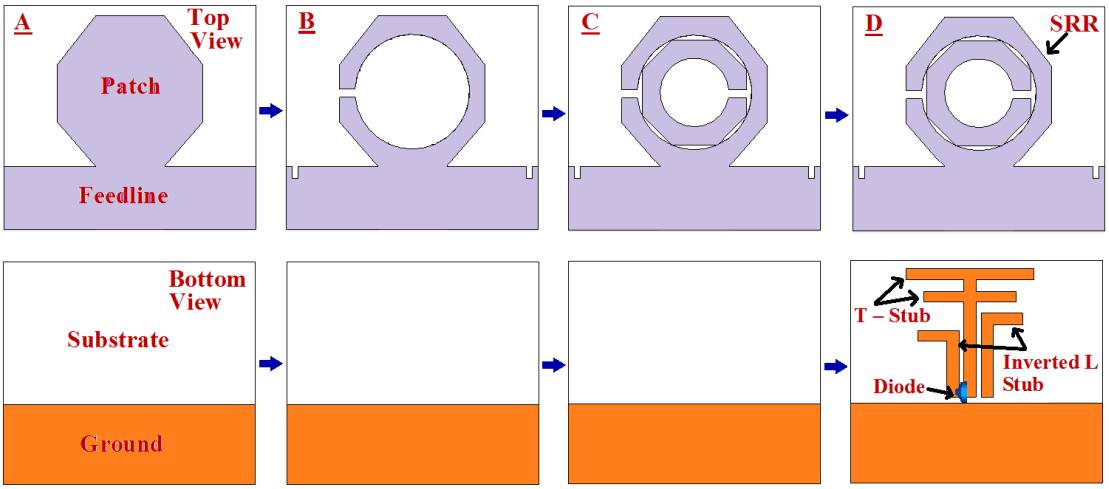

Figure 1. Design evolution steps of proposed multiband antenna.

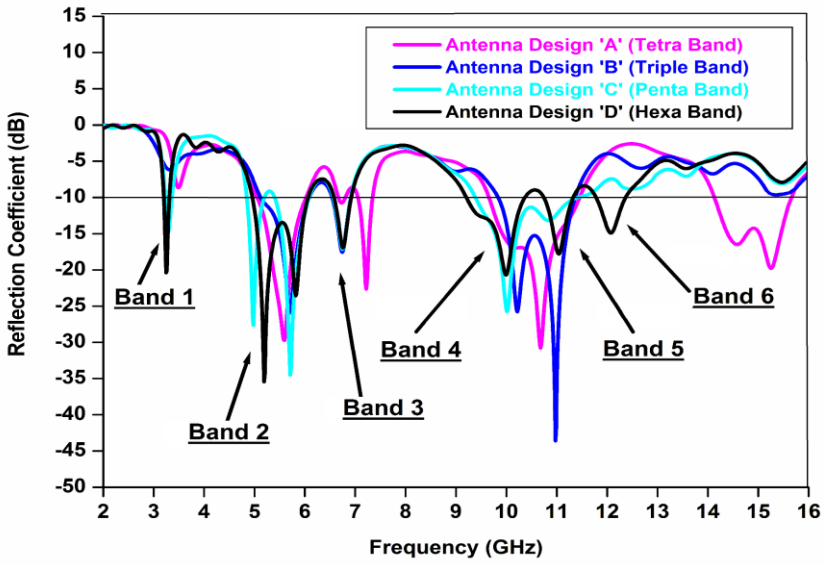

Figure 2. Simulated S_{11} of proposed antenna design ‘A’ to ‘D’.

International Journal of Engineering Research & Technology (IJERT)
ISSN: 2278-0181
Vol. 14 Issue 06, June - 2025

Table 1. Evolutionary Development Stages of the Proposed Antenna

Antenna Design Stages	Configuration of upper and lower part of antenna design	Operating band (in GHz)	Bandwidth (in %)	Modes of Wireless Applications achieved	Reasons
A	Upper section: Octagonal radiating section connected to a rectangular-shaped feedline Lower section: Defected rectangular Ground Structure (DGS)	Sim.: 5.06–6.02, 7.07–7.36, 9.67–11.48, 14.14–15.68	Sim.: 17.33, 4.02, 17.12, 10.33	No. of Applications – 4 Tetra band (5G Sub-6 GHz NR Bands, Upper C band, Upper X band and Lower K_U band wireless communication bands)	The tetra-band characteristics is achieved using an octagonal shape radiating patch combined with rectangular feedline and a rectangular -shaped Defected Ground Structure (DGS).
B	Upper section: Single octagonal shape radiating section connected to a slotted rectangular-shaped feedline Lower section: Defected rectangular Ground Structure (DGS)	Sim.: 5.09–6.10, 6.53–6.93, 9.84–11.41	Sim.: 18.05, 5.94, 14.78	No. of Applications – 3 Triple band (5G Sub-6 GHz NR Bands, Upper C band, Upper X band wireless communication bands)	The current perturbation effect is induced by the slotted single octagonal ring patch area and the inclusion of a slotted rectangular slotted feedline along with rectangular defected ground plane.
C	Upper section: double SRR based octagonal shape radiating section connected to a slotted rectangular-shaped feedline Lower section: Defected rectangular Ground Structure (DGS)	Sim.: 3.21–3.39, 4.84–5.19, 5.41–6.12, 6.56–6.94, 9.35–11.52	Sim.: 5.45, 6.98, 12.32, 5.63, 20.79	No. of Applications – 5 Penta band (5G Sub-6 GHz NR Bands, Upper S band, C band, and Upper X band)	The current perturbation effect is induced by the slotted double octagonal SRR based patch and the inclusion of a slotted rectangular slotted feedline along with rectangular defected ground plane.
D	Upper section: Upper section: double SRR based octagonal shape radiating section connected to a slotted rectangular-shaped feedline	Sim.: 3.16–3.34, 4.94–6.10, 6.57–6.94, 9.16–10.35, 10.71–11.32, 11.76– 12.36	Sim.: 5.54, 21.01, 5.48, 12.19, 5.54, 4.98	No. of Applications – 6 Hexa band	The current perturbation effect is induced by the slotted double octagonal SRR based patch and the inclusion of a slotted rectangular slotted feedline along with rectangular defected ground plane loaded with double inverted L-shaped and single T-shaped stubs.

International Journal of Engineering Research & Technology (IJERT)
ISSN: 2278-0181
Vol. 14 Issue 06, June - 2025

	Lower section: Defected rectangular Ground Structure (DGS) loaded with two inverted L-shaped and single T- shaped stubs			(5G Sub-6 GHz NR Bands, Upper S band WiMAX, Lower C band WLAN, Upper C band, Lower X band, Upper X band, and Lower K_U band)	

The proposed design is designed on a 1.6 mm thick FR4 substrate (44 × 39 × 1.6 mm³) with a relative permittivity of 4.3 and a loss tangent of 0.02, featuring a vertex-fed configuration. The top side consists of an octagonal split-ring resonator (SRR) as the radiating element, integrated with a slotted rectangular feedline, while the bottom side includes a rectangular ground plane equipped with two inverted L-shaped stubs and one T-shaped stub. As illustrated in Figure 3, the octagonal SRR comprises two conductive rings with circular slots of radii r_1 and r_2, with opposing etched slits. The inverted L-shaped stubs and the T-shaped stub, along with a diode (D), are embedded within the ground section. Figure 3 provides a detailed view of the proposed antenna, showcasing its top, side, and bottom views. The optimized dimensions of the proposed multiband antenna are:- L_S = 44 mm, W_S = 39 mm, h = 1.6 mm, r_1 = 6 mm, r_2 = 10 mm, a_1 = 8 mm, a_2 = 10 mm, W_F = 11 mm, t_1 = 1.5 mm, W_G = 14 mm, L_{SL} = 1 mm, W_{SL} = 2 mm, L_1 = 22 mm, L_2 = 16 mm, L_3 = 7 mm, W_1 = 2 mm, L_{g1} = 23 mm, L_{g2} = 19 mm, L_{g3} = 12 mm, g_1 = 2 mm and g_2 = 7 mm.

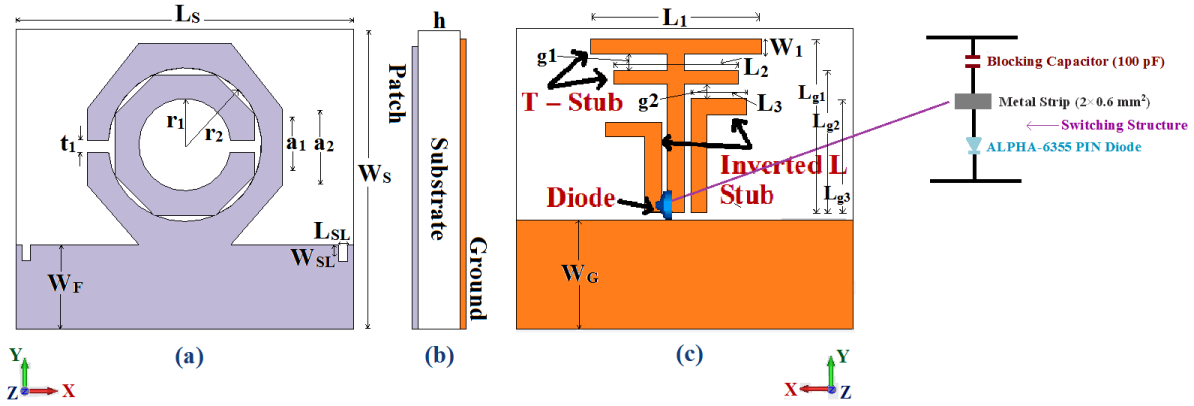

Figure 3. Proposed Antenna Configuration: (a) Front view, (b) Side view, (c) Back view of the structure.

The switching operation of the PIN diode is facilitated by applying DC voltage to a conductive metal strip, measuring 2×0.6 mm², positioned between the T-shaped and inverted L-shaped stubs in the ground plane, as illustrated in Figure 3. A 100 pF blocking capacitor is placed within the slot to establish the RF connection for the PIN diode while isolating the RF signal from the DC voltage. The beam-lead PIN diode (ALPHA-6355), characterized by extremely low capacitance during biasing, is connected to the metal strip within the slot [34]. The diode is biased by applying a 0.7 V DC voltage to the metal strip. In this forward-biased (ON) state, the diode exhibits a resistance of 2.6 Ω. When the DC voltage is absent, the diode enters the reverse-biased (OFF) state, displaying a capacitance of 0.081 pF. In the forward-biased state, the metal strip effectively connects to the ground plane, becoming an integral part of it. The RF equivalent circuit of the diode in the forward-biased (ON) state is modeled as a series connection of a current-controlled resistor (R_{CC}) and a fixed inductor (L_F), as illustrated in Figure 4(a). In the reverse-biased (OFF) state, the equivalent circuit is represented as a shunt combination of a resistor (R_{CC}) and a reactive capacitor (C_R) in series with a fixed inductor (L_F), as depicted in Figure 4(b). The intrinsic-layer capacitor (C_R) and shunt resistor (R_{CC}) are influenced by the diode's depletion layer. The reactive capacitor (C_R) is composed of the stray capacitance (C_S) and the junction capacitance (C_J). The stray capacitance (C_S) arises due to the structural effects of the diode's packaging.

International Journal of Engineering Research & Technology (IJERT)
ISSN: 2278-0181
Vol. 14 Issue 06, June - 2025

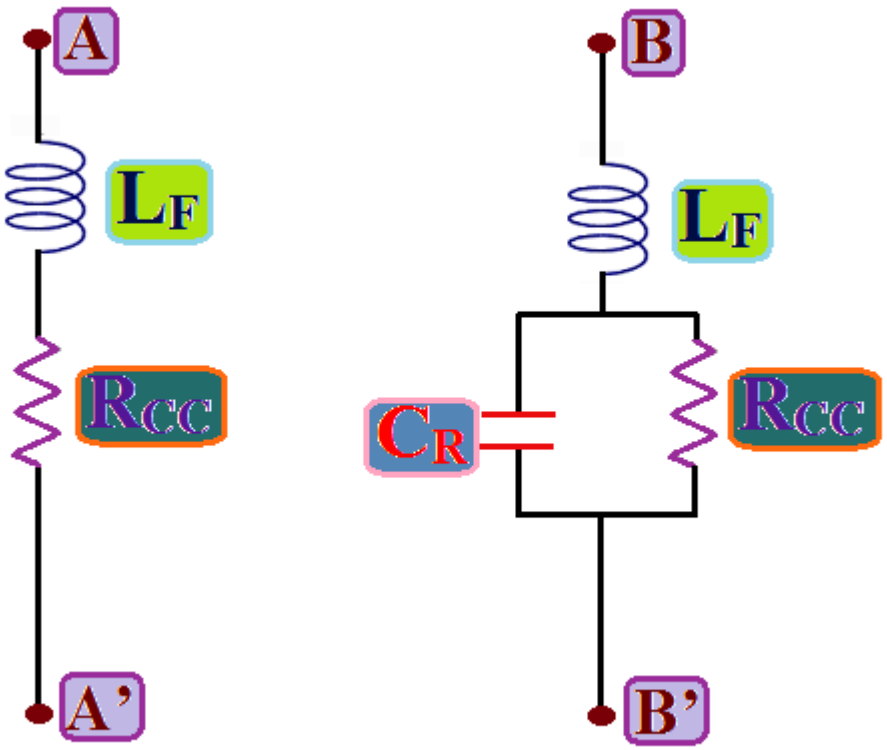

(a) (b)

Figure 4. Equivalent circuit for PIN diode: (a) Forward bias (ON-state), (b) Reverse bias (OFF-state).

The resulting six excited modes are observed at 3.3, 5.8, 6.8, 9.9, 11.01, and 12.05 GHz for various eigenvalues. These modes differ from those commonly utilized in standard wireless applications. The impedance matching for these resonant modes is achieved by incorporating an SRR-based radiating element and a reclined L-shaped slot in the ground plane of the antenna structure. The input impedance of the microstrip antenna is determined by analyzing the electromagnetic fields between the patch and the ground plane. This impedance can be expressed as a series of resonant modes, where each radiating mode is modeled as a general parallel RLC circuit with an equivalent input impedance [35]. The input impedance of the equivalent circuit at the feed point of the antenna is expressed as:

$$Z_{equv}(f) = j\,2\pi f\,L_{\infty} + \sum_{i=1}^{M} [\,R_{r,i} / (1+j)\,Q_{u,i}\;\{(f / f_{r\text{-}i})\,(f_{r\text{-}i} / f)\}\,] \quad (1)$$

where Z_{equv} is the input impedance of the equivalent circuit at the antenna's feed point, L_{∞} represents the feed point impedance at higher frequency bands, M is the total number of radiating resonances within the operating band, and $f_{r,i}$, $Q_{u,i}$ and $R_{r,i}$ denote the resonance frequency, Q-factor, and radiation resistance of the i^{th} radiating mode, respectively. The equivalent circuit representation is depicted in Figure 5.

International Journal of Engineering Research & Technology (IJERT)
ISSN: 2278-0181
Vol. 14 Issue 06, June - 2025

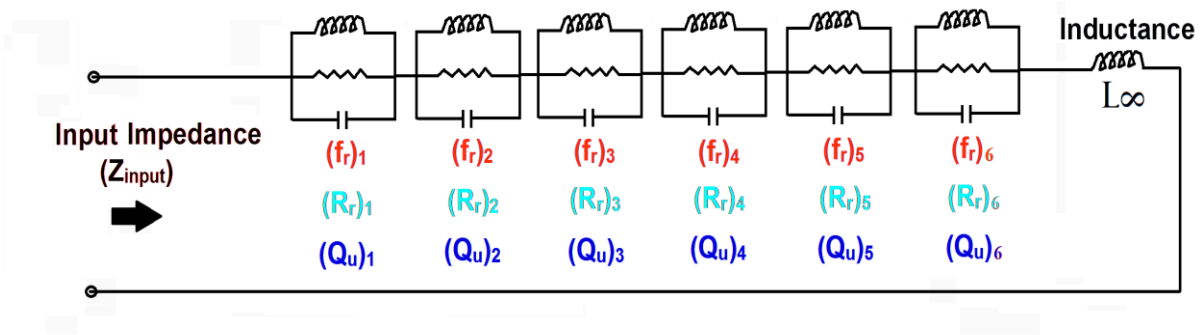

Figure 5. Topology of equivalent model for proposed multiband antenna.

The tunability of the antenna across various wireless standards is achieved by modifying the state of the PIN diode. When the PIN diode is in the ON state, the gap between the inverted L-shaped stub and the T-shaped stub in the ground plane is bridged, enabling support for additional wireless communication standards. Conversely, in the OFF state, the antenna exhibits hexa-band characteristics, covering a range of wireless communication applications [36]. The desired hexa-band performance of the proposed design is realized by switching the PIN diode between ON and OFF states. In the ON state, the extended current path supports penta-band resonant modes at 5.21, 6.76, 9.93, 11.11, and 12.10 GHz, as shown in Figure 6. In the OFF state, variations in the antenna's current path enable hexa-band operation. The impedance bandwidths for the OFF state are 5.54% (3.16–3.34 GHz), 21.01% (4.94–6.10 GHz), 5.48% (6.57–6.94 GHz), 12.19% (9.16–10.35 GHz), 5.54% (10.71–11.32 GHz), and 4.98% (11.76–12.36 GHz). For the ON state, the impedance bandwidths are 20.53% (4.94–6.07 GHz), 5.17% (6.59–6.94 GHz), 12.07% (9.26–10.45 GHz), 5.67% (10.79–11.42 GHz), and 4.98% (11.76–12.36 GHz), as depicted in Figure 8. The proposed design provides adequate bandwidth to meet the requirements of various wireless standards while enabling frequency band reconfiguration. Comparative S-parameter (S_{11}) plots for forward and reverse bias states are presented in Figure 6. The simulated data was generated using CST Microwave Studio (MWS) software [33], accounting for different PIN diode states. In practice, the operation of the PIN diode requires a biasing circuit to apply forward or reverse bias.

International Journal of Engineering Research & Technology (IJERT)
ISSN: 2278-0181
Vol. 14 Issue 06, June - 2025

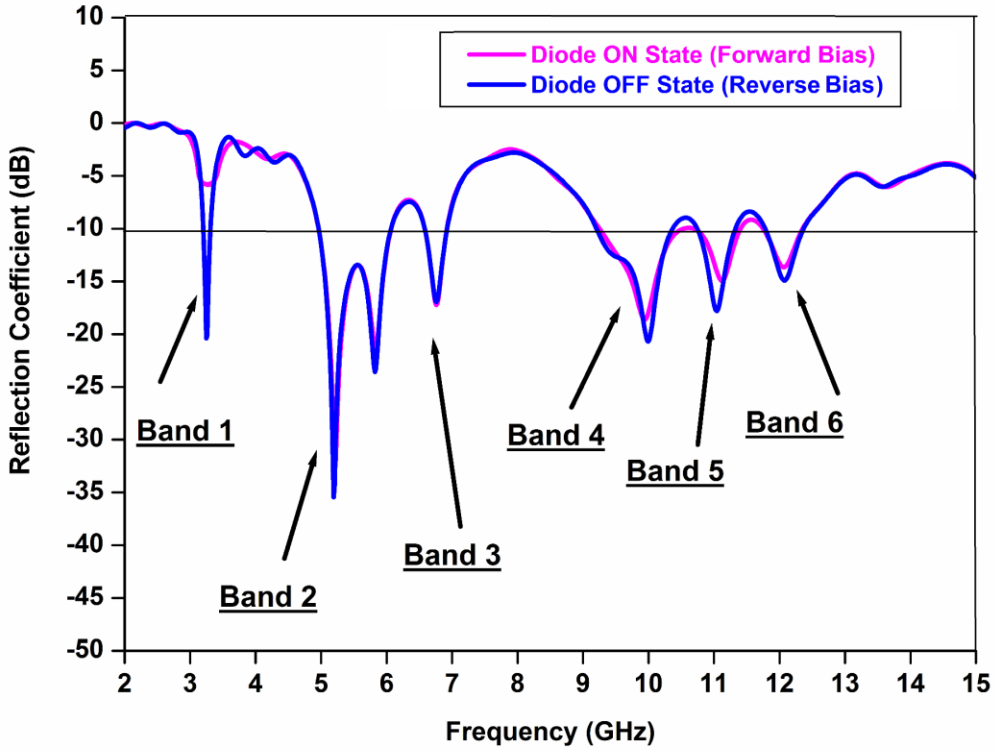

Figure 6. Simulated S_{11}: ON and OFF State of PIN Diode.

3. PARAMETRIC OBSERVATION

The operational performance of the proposed antenna is analyzed by varying key parameters, including feedline width (W_F), ground width (W_G), slot width of the SRR-based octagonal ring (t_1), feedline slot width (W_{SL}), and feedline slot length (L_{SL}). This parametric study examines the impact of these variations while keeping all other parameters constant, as illustrated in Figures 7–12. For Cases 1, 2, and 3, the parameters W_F, W_G, and t_1 are varied within the ranges of 10.5–12.0 mm, 12.0–15.0 mm, and 0.5–3.5 mm, respectively, as shown in Figures 7–9. The results indicate that changes in these parameters significantly affect the reflection coefficient (S_{11}) and the corresponding frequency bands. At lower frequencies, reductions in W_F, W_G, or t_1 impact the lower frequency bands (Bands 1 and 2), causing frequency shifts at higher bands (Bands 3, 4, 5, and 6). Optimized impedance matching and hexa-band characteristics are achieved at W_F = 11.0 mm, W_G = 14.0 mm and slot width t_1 = 1.5 mm. As observed in Figures 7–9, impedance matching improves across the operating frequency bands when feedline width (W_F), ground width (W_G) and slot width (t_1) increases. Conversely, a decrease in W_F, W_G, or t_1 results in degraded impedance matching and shifts in frequency bands. This parametric analysis underscores the importance of precise dimensional optimization to achieve the desired antenna performance and hexa-band characteristics.

International Journal of Engineering Research & Technology (IJERT)
ISSN: 2278-0181
Vol. 14 Issue 06, June - 2025

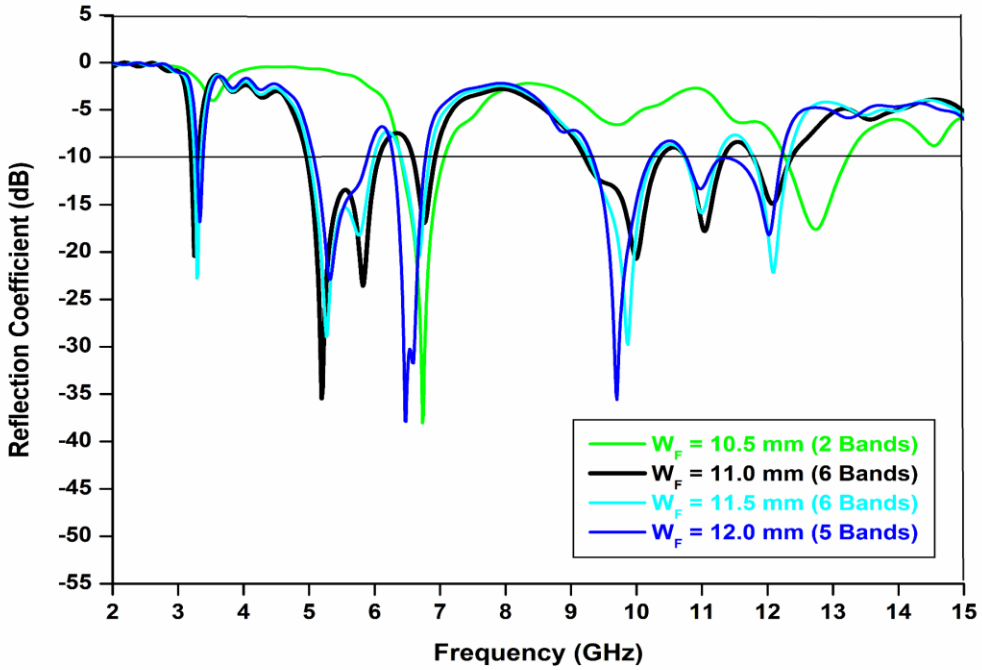

Figure 7. Parametric observations: feedline width W_F Variations.

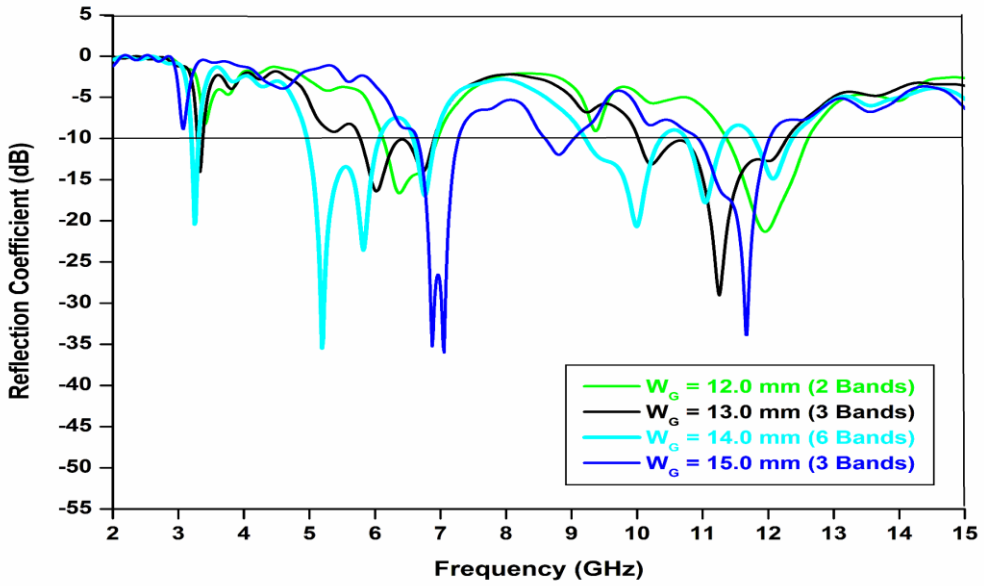

Figure 8. Parametric observations: ground width W_G Variations.

International Journal of Engineering Research & Technology (IJERT)
ISSN: 2278-0181
Vol. 14 Issue 06, June - 2025

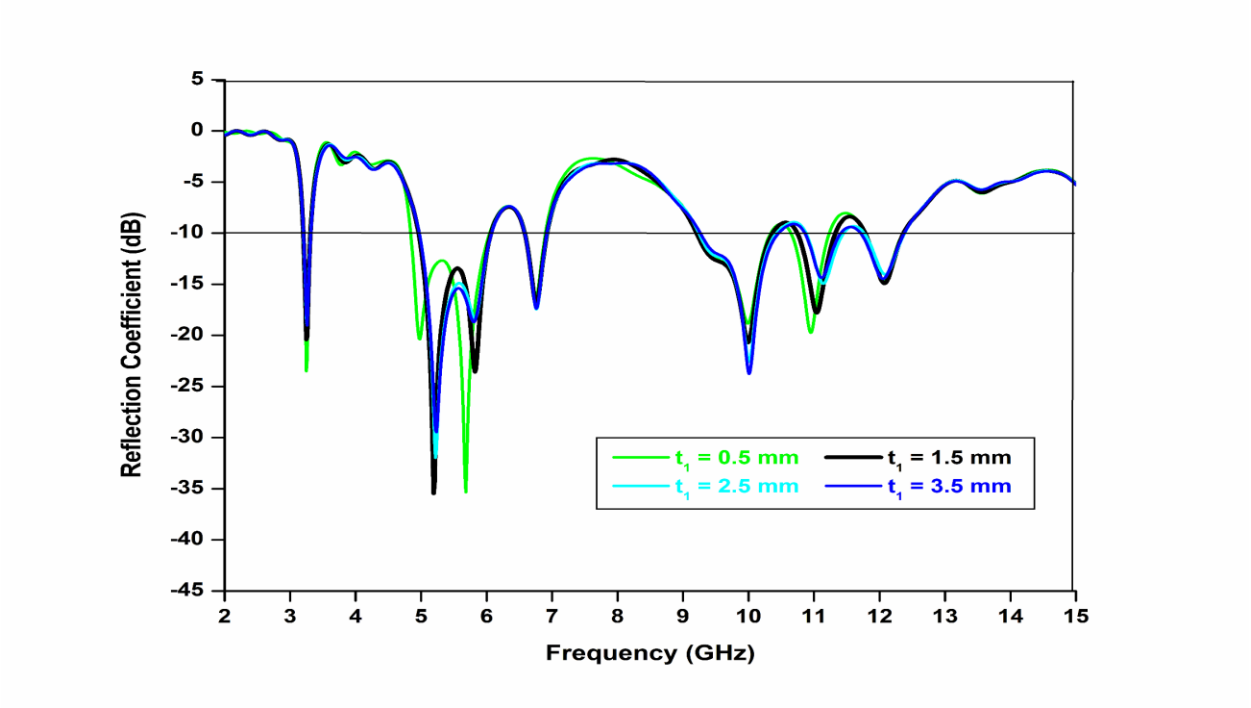

Figure 9. Parametric observations: slot width t_1 Variations.

For cases 4 and 5, the feedline slot dimensions W_{SL} and $L_{SL}$are varied within the ranges of 1–4 mm and 0.5–2.0 mm, respectively, as depicted in Figures 10–11. The results indicate that variations in these dimensions have a notable impact on the resulting frequency bands. Specifically, as W_{SL} increases in 1 mm increments, the number of frequency bands suitable for wireless applications decreases. The optimal hexa-band configuration, with an input reflection coefficient (S_{11}) below -10 dB, is achieved at W_{SL} = 2 mm and L_{SL} = 1.0 mm. From Figures 10 and 11, it is evident that, the impedance matching across the operating bands improves as the feedline slot dimensions increase. The observed changes in frequency bands with variations in W_{SL} and L_{SL} highlight the importance of selecting optimal values for these parameters to achieve the best antenna performance. This study demonstrates that careful tuning of feedline slot dimensions is crucial for ensuring robust hexa-band characteristics and maintaining consistent impedance matching across the frequency bands.

International Journal of Engineering Research & Technology (IJERT)
ISSN: 2278-0181
Vol. 14 Issue 06, June - 2025

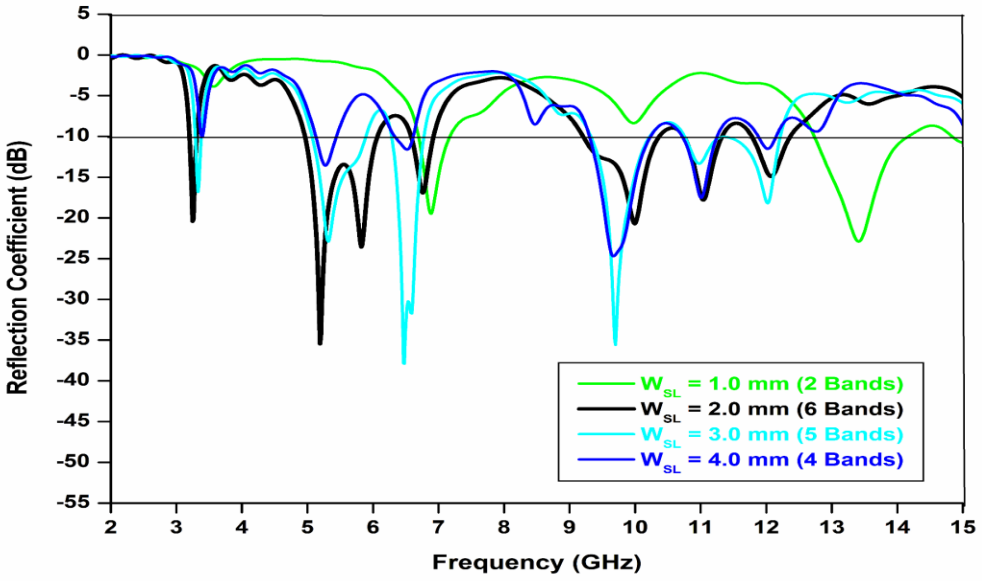

Figure 10. Parametric observations: feedline slot width W_{SL} Variations.

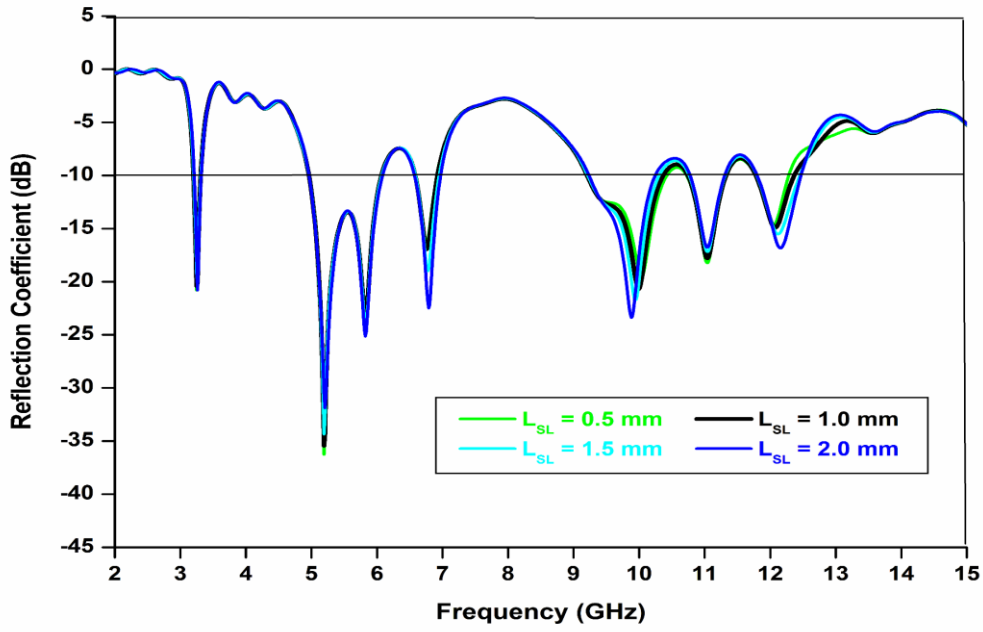

Figure 11. Parametric observations: feedline slot length L_{SL} Variations.

International Journal of Engineering Research & Technology (IJERT)
ISSN: 2278-0181
Vol. 14 Issue 06, June - 2025

4. RESULTS AND DISCUSSION

The simulated surface current distributions of the proposed antenna at its resonant frequencies 3.27 GHz, 5.0 GHz, 6.76 GHz, 9.98 GHz, 11.01 GHz, and 12.07 GHz are shown in Figure 12. At the lower resonant frequency of 3.27 GHz (WiMAX), the surface currents are predominantly distributed along the outer periphery of the outer octagonal ring of the radiating element. For the upper WLAN frequency band at 5.0 GHz, the surface currents concentrate heavily around the inner octagonal SRR radiating element, enhancing impedance matching and narrowing the bandwidth at this frequency. Notably, as the frequency increases, the current distribution shifts from the outer ring toward the inner ring of the antenna structure. At 6.76 GHz (Upper C-band), which is used for long-distance radio telecommunications, and at 9.98 GHz (Lower X-band) for satellite communications, the surface current is maximally concentrated around the slotted rectangular feedline. For the higher resonant frequencies at 11.01 GHz (Upper X-band) and 12.07 GHz (Lower Ku-band), surface currents are strongly concentrated near the T-shaped and inverted L-shaped stubs in the ground plane. These distributions contribute to the antenna's functionality for applications like amateur radio and molecular rotational spectroscopy, respectively.

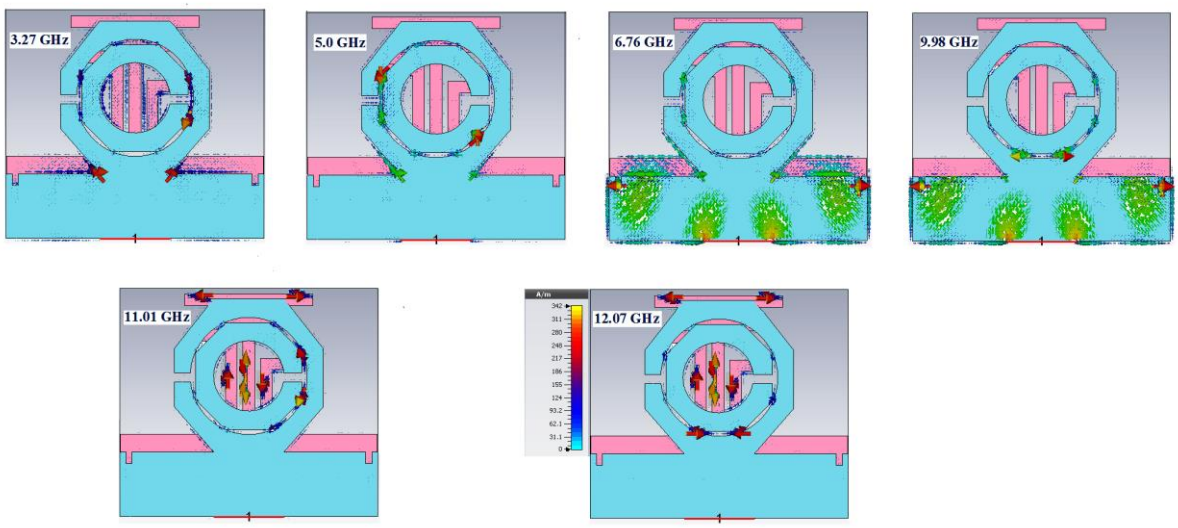

Figure 12. Current distribution at resonant frequencies (3.27 GHz, 5.0 GHz, 6.76 GHz, 9.98 GHz, 11.01 GHz, and 12.07 GHz).

The proposed design demonstrates a simulated peak gain of 2.72 dB, 3.89 dB, 2.92 dB, 2.88 dB, 3.29 dB, 3.54 dB, and 4.14 dB at the wireless standards of 3.27 GHz, 5.0 GHz, 5.8 GHz, 6.76 GHz, 9.98 GHz, 11.01 GHz, and 12.07 GHz, respectively, as shown in Figure 13. Similarly, Figure 14 illustrates the simulated radiation efficiencies of 68.25%, 74.72%, 78.79%, 79.65%, 81.68%, 83.45%, and 87.88% at these frequencies.

International Journal of Engineering Research & Technology (IJERT)
ISSN: 2278-0181
Vol. 14 Issue 06, June - 2025

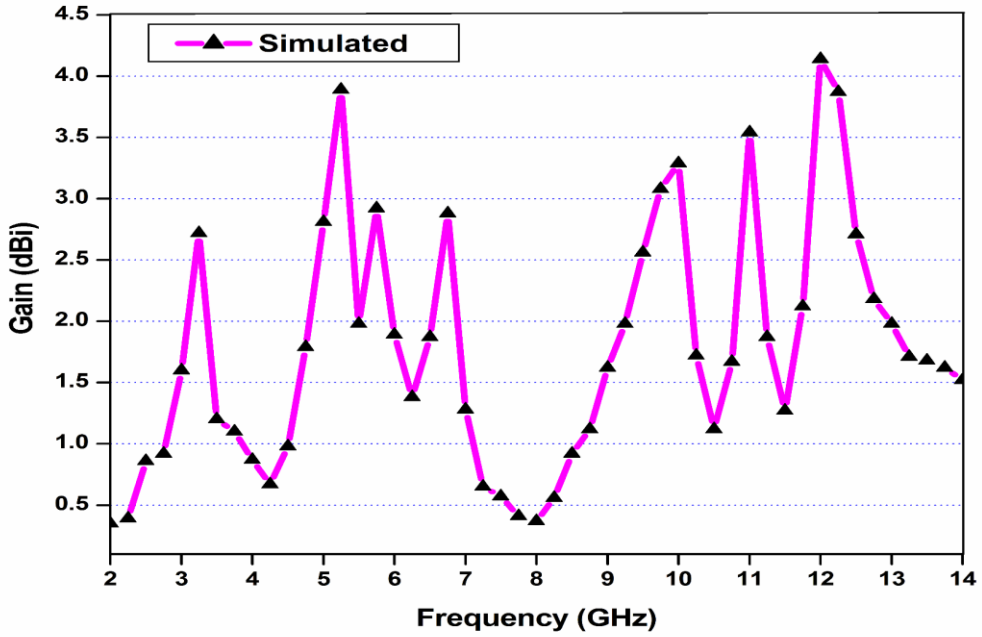

Figure 13. Antenna gain of the proposed design in simulated mode.

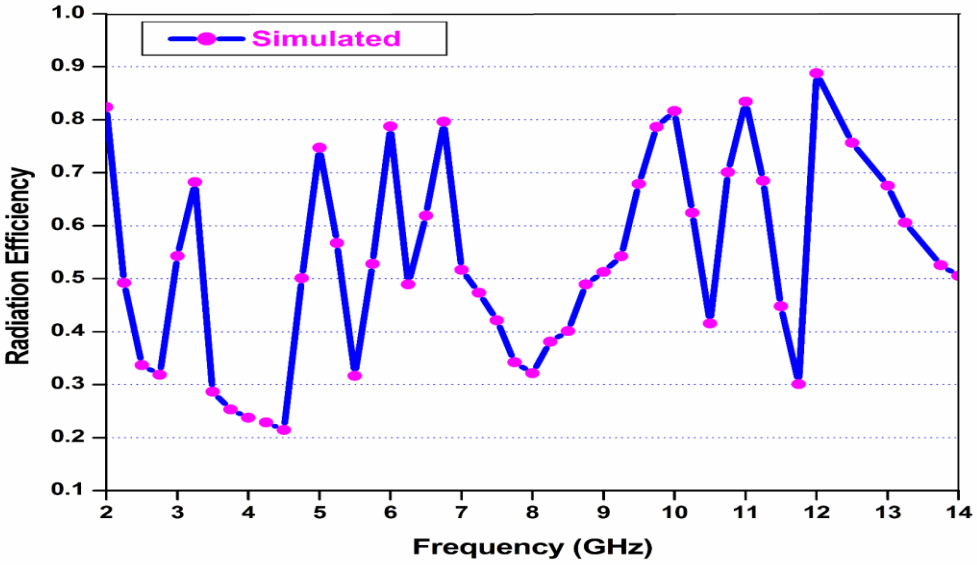

Figure 14. Radiation efficiency of the proposed design in simulated mode.

International Journal of Engineering Research & Technology (IJERT)
ISSN: 2278-0181
Vol. 14 Issue 06, June - 2025

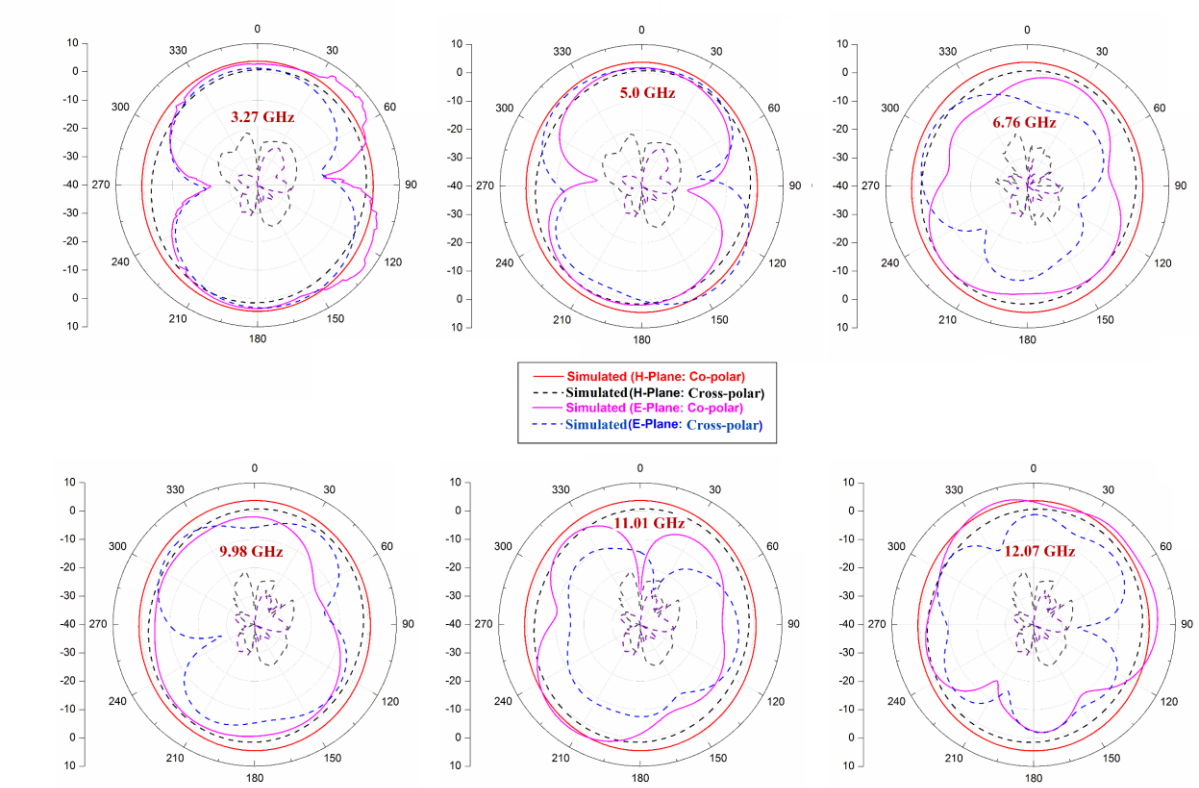

Figure 15. E and H plane co-polar and cross-polarization radiation patterns at resonant frequencies (3.27 GHz, 5.0 GHz, 6.76 GHz, 9.98 GHz, 11.01 GHz, and 12.07 GHz).

Figure 15 presents a comparison of the radiation patterns obtained from simulations and experimental measurements for the E- and H-planes (co-polarization and cross-polarization) of the proposed design, showing good agreement. The patterns are analyzed at frequencies of 3.27 GHz, 5.0 GHz, 6.76 GHz, 9.98 GHz, 11.01 GHz, and 12.07 GHz. The E-plane exhibits dipole-like radiation patterns, while the H-plane demonstrates omnidirectional characteristics, highlighting the suitability of the proposed design for wireless communication applications. Additionally, the patterns show low cross-polarization levels (less than –15 dB) across all resonant frequency modes. Consistent omnidirectional radiation is observed in the H-plane, while the E-plane displays nearly bi-directional patterns in both co-polarization and cross-polarization modes at all operating frequencies.

Table 2 provides a comparative analysis of the proposed antenna's characteristics, including its size, impedance bandwidth, gain, radiation efficiency, and the number of operating modes, against other reported multiband antennas designed for wireless standards.

International Journal of Engineering Research & Technology (IJERT)
ISSN: 2278-0181
Vol. 14 Issue 06, June - 2025

Table 2: Comparison of the proposed design with state-of-the-art literature.

Ref	Year	Antenna Dimension (in mm^3)	Bandwidth (in %)	Gain (in dBi)	Radiation Efficiency (in %)	No. of Resonating Modes (in GHz)	Achieved Wireless Applications	Frequency Band Reconfig-urability established
[10]	2013	52.6×30×1	47.27/38.88	-0.56/-0.62	89.2/98.1	2	GPS/WLAN (1.5/2.4)	No
[7]	2015	56×44×0.8	5.56/5.86/19.34/ 13.69	1.3/2.3/3.5/4. 4	76.8/80.1/96.6/85. 5	4	GPS/WLAN/ WiMAX (1.5/2.4/3.5/ 5.4)	No
[11]	2018	32×38×1.6	8/6/5/69.3	3.8 (Avg. Gain)	89% (Avg. Rad. Eff.)	4	WLAN/ WiMAX/ITU/X Band (2.4/3.35/5.8/7.5)	No
[13]	2019	44 × 39 × 1.6	5.11/7.33/11.70/ 6.38/12.03/5.62	2.72/3.81/2.1 2/2.78/3.68/4. 10	41.2/84.7/52.8/69. 7/78.8/76.9	6	WLAN/WiMAX/ C/X /Ku Band (3.3/5.0/5.8/6.6/9.9/ 15.9)	Yes
[37]	2020	25×25×1.6	7.7/6.51/6.49/8. 61/4.94	2/2.9/2.5/4.42 /3.01	--	5	IoT/WLAN/ Wi-Max/ C-band (3.82/4.11/4.48/ 4.90/6.04)	Yes
[29]	2021	150×150×1.5 2	40	4.91 (Max. peak Gain)	--	1	S band (2.0 – 3.0 GHz)	
[30]	2022	28×25×1.53	16.76/ 15.38/ 83.07/ 43.03/ 44.30/ 28.69	1.6/ 1.8/ 5.8/ 2.3/ 1.9/ 2.5	91.3/ 93.4/ 86.8/ 87.5/ 89.7/ 89.3	6	WLAN/Bluetooth (2.4-2.5 GHz), Aeronautical Radio Navigations (2.7-2.9 GHz), WLAN (5.0-6.0 GHz), Wi-MAX (3.3-3.8 GHz), INSAT C-band Applications (6.72-7.02 GHz), X-band Satellite communication (7.9-8.4 GHz), International Telecommunication Union Fixed wireless system (ITU) (7.725-8.4 GHz)	Yes
[31]	2023	42×30×1.6	22.09/ 9.56	1.4/ 3.3	--	2	GPS/RADAR (1.8 GHz) / WLAN (5.2 GHz)	Yes
[32]	2023	41×44×1.52	3.8/ 5.2	4.84/ 6.01	92.5/ 91.8	2	WBAN (ISM 2.4 GHz and 5.8 GHz)	Yes
Proposed antenna		44 × 39 × 1.6	5.54/ 21.01/ 5.48/ 12.19/ 5.54/ 4.98	2.72/ 3.89/ 2.88/ 3.29/ 3.54/ 4.14	68.25/ 74.72/ 79.65/ 81.68/ 83.45/ 87.88	6	S band WiMAX, WLAN / Upper S band (WiMAX) / Lower C band (WLAN)/ 5G NR bands (n46: 5.15-5.925 GHz, n47: 5.855-5.925 GHz) / Upper C band (long distance radio telecommunication)/ Lower X band (satellite communication) / Upper X band (amateur radio applications) / Lower Ku band (molecular	Yes

International Journal of Engineering Research & Technology (IJERT)
ISSN: 2278-0181
Vol. 14 Issue 06, June - 2025

							rotational spectroscopy) (3.27, 5.0/ 5.8, 6.76, 9.98, 11.01, 12.07)	

5. CONCLUSION

This paper presents an SRR-based stub-loaded multiband antenna designed for a range of wireless standards, including the Upper S band (WiMAX: 3.3 GHz), Lower C band (WLAN: 5.0/5.8 GHz), 5G Sub-6 GHz NR bands (n46 and n47), Lower X band (9.98 GHz for satellite communication), Upper X band (11.01 GHz for amateur radio), and Lower Ku band (12.07 GHz for molecular rotational spectroscopy applications. The radiating element features octagonal-shaped split rings attached to a rectangular slotted feedline, which imparts the multiband characteristics. To achieve hexa-band functionality, inverted L-shaped and T-shaped stubs with a PIN diode are incorporated into the ground plane. The radiation characteristics of the proposed antenna show good impedance matching across these resonant frequencies. Fabricated on a low-cost FR4 dielectric substrate, the design enables easy integration with wireless terminal devices. The antenna demonstrates consistent radiation patterns, gain, and efficiency across all operating bands, making it a promising option for wireless applications. The use of a PIN diode in the stubs at the defected ground plane allows for frequency band reconfigurability, enhancing the versatility of the proposed design.

REFERENCES

[1] Agiwal, M., A. Roy, and N. Saxena, “Next generation 5G wireless networks: A comprehensive survey,” IEEE Commun. Surv. Tutorials, Vol. 18, No. 3, pp. 1617–1655, 2016.

[2] 3G PP specification series: 38 series. Online Available: https://www.3gpp.org/Dyna Report/38-series.htm, 2020.

[3] Jin, G., C. Deng, Y. Xu, J. Yang, and S. Liao, “Differential frequency-reconfigurable antenna based on dipoles for sub-6 GHz 5G and WLAN applications,” IEEE Antennas Wirel. Propag. Lett., Vol. 19, No. 3, pp. 472– 476, 2020.

[4] Zeng, J., and K.M. Luk, “Single-layered broadband magnetoelectric dipole antenna for new 5G application,” IEEE Antennas Wirel. Propag. Lett., Vol. 18, No. 5, pp. 911–915, 2019.

[5] Sim, C. Y. D., H. Y. Liu, and C.J. Huang, “Wideband MIMO antenna array design for future mobile devices operating in the 5G NR frequency bands n77/n78/n79 and LTE band 46,” IEEE Antennas Wirel. Propag. Lett., Vol. 19, No. 1, pp. 74–78, 2020.

[6] Wu, R.Z., P. Wang, Q. Zheng, and R.P. Li, “Compact CPW-fed triple band antenna for diversity applications,” Electron Letters, Vol. 51, pp. 735–736, 2015.

[7] Cao, Y.F., S.W. Cheung, and T.I. Yuk, “A Multiband Slot Antenna for GPS/WiMAX/WLAN Systems,” IEEE transactions on antennas and propa., Vol. 63, No. 3, pp. 952-958, 2015.

[8] Saraswat, R.K., and M. Kumar, “A Frequency Band Reconfigurable UWB Antenna for High Gain Applications,” Progress In Electromagnetics Research B, Vol. 64, pp. 29–45, 2015.

[9] Ali, T., S. Pathan, and R.C. Biradar, “A multiband antenna loaded with metamaterial and slots for GPS/WLAN/WiMAX applications,” Micro. and Opt. Techno. Lett., Vol. 60, pp. 79–85, 2018.

[10] Xu, H.X., G.M. Wang, Y.Y. Lv, M.Q. Qi, X. Gao, and S. Ge, “Multi frequency monopole antennas by loading metamaterial transmission lines with dual-shunt branch circuit,” Progress In Electromagnetics Resear. Vol 137, pp. 703–725, 2013.

[11] Rao, M.V., B.T.P. Madhav, T. Anilkumar, and B.P. Nadh, “Metamaterial Inspired Quad Band Circularly Polarized Antenna for WLAN/ISM/Bluetooth/WiMAX and Satellite Communication Applications,” AEU-Int. J. of Electro. and Comm., Vol. 97, pp. 229–241, 2018.

[12] Saraswat, R.K., and M. Kumar, “Miniaturized Slotted Ground UWB Antenna Loaded with Metamaterial for WLAN and WiMAX Applications,” Prog. In Electro. Res. B., Vol. 65, pp. 65–80, 2016.

[13] Saraswat, R.K., and M. Kumar, “A vertex-fed hexa-band frequency reconfigurable antenna for wireless applications,” Int. J. RF Microw. Comput. Aided Eng., Vol. 29, No. 10, pp.1–13, 2019.

[14] Saraswat, R.K., and M. Kumar, “A Quad Band Metamaterial Miniaturized Antenna for Wireless Applications with Gain Enhancement,” Wireless Personal Communications, Vol. 114, 3595-3612, 2020.

[15] Saraswat, R.K., and M. Kumar, “Implementation of hybrid fractal metamaterial inspired frequency band reconfigurable multiband antenna for wireless applications,” Int. J. RF Microw. Comput. Aided Eng., Vol. 30, No. 9, 1–19, 2020.

[16] Mu, W., Z. Wang, M. Yang, W. Nie, and P. Wang, “A Six-Port Slot Antenna System with Wideband and High-Isolation for 5G NR Bands,” Prog. In Electro. Res. M., Vol. 107, pp. 105–118, 2022.

[17] Murugan, C., and T. Kavitha, “A Compact Four-Element Modified Annular Ring Antenna for 5G Applications,” Prog. In Electro. Res. C., Vol. 137, pp. 169–183, 2023.

International Journal of Engineering Research & Technology (IJERT)
ISSN: 2278-0181
Vol. 14 Issue 06, June - 2025

[18] Agrawal, A., and J. Vaswani, "A Four Port, Dual Band Antenna for Fifth Generation Mobile Communication and WLAN Services," ACTA TECHNICA CORVINIENSIS – Bulletin of Engineering, Vol. 4, 73-76, 2020.
[19] Agrawal, A., and J. Vaswani, "Twelve-Port Dual-Polarized Dual-Band MIMO Antenna for Fifth generation Mobile Devices," ICTACT Journal on Communication Technology, Vol. 12, No. 3, 2490-2497, 2021.
[20] Agrawal, A., and J. Vaswani, "Dual-Band, Dual-Polarized Two Element Slot Antenna for Fifth Generation Mobile Devices," Turkish J. Comput. Maths. Educ, Vol. 12, No. 3, 4822-4830, 2021.
[21] Rajeshkumar, V., and S. Raghavan, "A compact metamaterial inspired triple band antenna for reconfigurable WLAN/WiMAX applications," Int. J. Electron. Commun., Vol. 69, No. 1, 274–280, 2015.
[22] Agrawal, A., P. K. Singhal, and A. Jain, "Design and optimization of a microstrip patch antenna for increased bandwidth," International Journal of Microwave and Wireless Technologies, Vol. 5, No. 4, 529-535, 2013.
[23] Puri, I., and A. Agrawal, "Bandwidth and Gain increment of microstrip patch Antenna with Shifted elliptical Slot," International Journal of Engineering Science and Technology, Vol. 3, No. 7, 5539-5545, 2011.
[24] Shagun, A. Agrawal, and Priyanka "CPW-fed Wideband Antenna with U-shaped Ground Plane," International Journal of Wireless and Microwave Technologies, Vol. 5, 25-31, 2014.
[25] Jain, A., and A. Agrawal, "Design and optimization of a Microstrip patch Antenna for increased bandwidth," International Journal of Electronics and Communication Engineering, Vol. 7, No. 2, 191-195, 2014.
[26] Agrawal, A., M. Kumar, P. Jain, and S. Maheswari, "Tapered Circular Microstrip Antenna with Modified Ground Plane for UWB Communications," International Journal of Electronics and Communication Engineering & Technology (IJECET), Vol. 4, No. 3, 43-47, 2013.
[27] Singh, R.K., A. Basu and S.K. Koul, "Reconfigurable Microstrip Patch Antenna with Switchable Polarization," IETE Journal of Research, Vol. 66, No. 5, 1–10, 2018.
[28] Priya, A., and S.K. Mohideen, "Design of Frequency and Polarization Agile Patch Antenna for Wireless Communications," IETE Journal of Research, Vol. 68, No. 5, 1–12, 2020.
[29] Muthuvel, S.K., and Y. K. Choukiker, "Wideband Frequency Agile and Polarization Reconfigurable Antenna for Wireless Applications," IETE Journal of Research, Vol. 69, No. 3, 1–10, 2021.
[30] Mudda, S., K.M. Gayathri, and M. Mudda, "Wide-Band Frequency Tunable Antenna for 4G, 5G/Sub 6 GHz Portable Devices and MIMO Applications," Progress In Electromagnetics Research C, Vol. 118, 25-41, 2022.
[31] Pandhare, R.A., M.P. Abegaonkar, and C. Dhote, "High Gain Compact Dual Band Reconfigurable Antenna Using Multilayer FSS for WLAN and RADAR Applications," Progress In Electromagnetics Research C, Vol. 130, 227-240, 2023.
[32] Musa, U., S. M. Shah, Huda A. Majid, M. K. A. Rahim, M. S. Yahya, Z. Yunusa, A. Salisu, and Z. Z. Abidin, "Wearable Dual-Band Frequency Reconfigurable Patch Antenna for WBAN Applications," Progress In Electromagnetics Research M, Vol. 120, 95-111, 2023.
[33] Computer simulation technology microwave studio (CST MWS). Retrieved from http://www.cst.co.
[34] Alpha Industries. ALPHA-6355 beamlead PIN diode. Data sheet 2014 [Online]. Available: http://www.datasheetarchive.com/ALPHA/PINdiode6355-datasheet.html.
[35] Garg R., Bhartia P, Bahl I, Ittipiboon. Microstrip Antenna Design Handbook. Artech House, Boston, London; 2001.
[36] Saraswat, R.K., and M. Kumar, "A Frequency Band Reconfigurable UWB Antenna for High Gain Applications," Progress In Electromagnetics Research B, Vol. 64, 29–45, 2015.
[37] Singh, P.P., P.K. Goswami, S.K. Sharma, and G. Goswami, "Frequency Reconfigurable Multiband Antenna for IoT Applications in WLAN, Wi-Max, and C-Band," Progress In Electromagnetics Research C, Vol. 102, 149–162, 2020.